Computer Aided Geometric Design ••• (••••) •••–•••

Contents lists available at ScienceDirect

Computer Aided Geometric Design

www.elsevier.com/locate/cagd

Biomechanics simulations using cubic Hermite meshes with extraordinary nodes for isogeometric cardiac modeling

Adarsh Krishnamurthy [a,b,*], Matthew J. Gonzales [b], Gregory Sturgeon [c], W. Paul Segars [c], Andrew D. McCulloch [b]

[a] Mechanical Engineering, Iowa State University, United States
[b] Bioengineering, University of California, San Diego, United States
[c] Carl E. Ravin Advanced Imaging Laboratories, Duke University, United States

ARTICLE INFO

Article history:
Available online xxxx

Keywords:
Extraordinary nodes
Finite element analysis
Cubic-Hermite hexahedral elements
Cardiac modeling
Isogeometric analysis

ABSTRACT

Cubic Hermite hexahedral finite element meshes have some well-known advantages over linear tetrahedral finite element meshes in biomechanical and anatomic modeling using isogeometric analysis. These include faster convergence rates as well as the ability to easily model rule-based anatomic features such as cardiac fiber directions. However, it is not possible to create closed complex objects with only regular nodes; these objects require the presence of extraordinary nodes (nodes with 3 or $>= 5$ adjacent elements in 2D) in the mesh. The presence of extraordinary nodes requires new constraints on the derivatives of adjacent elements to maintain continuity. We have developed a new method that uses an ensemble coordinate frame at the nodes and a local-to-global mapping to maintain continuity. In this paper, we make use of this mapping to create cubic Hermite models of the human ventricles and a four-chamber heart. We also extend the methods to the finite element equations to perform biomechanics simulations using these meshes. The new methods are validated using simple test models and applied to anatomically accurate ventricular meshes with valve annuli to simulate complete cardiac cycle simulations.

1. Introduction

Computational models of cardiac biomechanics have been used to study normal cardiac physiology (Kerckhoffs et al., 2007) and pathological conditions such as heart failure (Kerckhoffs et al., 2010; Niederer et al., 2011). Advances in non-invasive imaging technology have made it feasible to generate patient-specific ventricular models (Aguado-Sierra et al., 2011; Krishnamurthy et al., 2013), but it remains difficult to create high-quality meshes that include anatomic features such as valve annuli automatically, owing to the irregular shape of the resulting cardiac geometry.

Cubic-Hermite finite element interpolation schemes have been popular in cardiac modeling because of their convergence properties in finite element simulations of ventricular biomechanics (Costa et al., 1996) and their ability to capture smooth geometries compactly. However, construction of cubic-Hermite geometric meshes has been limited to ventricular geometries below the valve plane due to difficulties in handling complex topologies of the atria and great veins (Fig. 2). Most previous cardiac models using high-order meshes have been restricted to geometries described by a single set of parametric coor-

* Corresponding author at: Mechanical Engineering, Iowa State University, United States.
E-mail addresses: adarsh@iastate.edu (A. Krishnamurthy), seventhsonmjg@gmail.com (M.J. Gonzales), gms19@duke.edu (G. Sturgeon), paul.segars@duke.edu (W.P. Segars), amcculloch@ucsd.edu (A.D. McCulloch).

http://dx.doi.org/10.1016/j.cagd.2016.02.016
0167-8396/

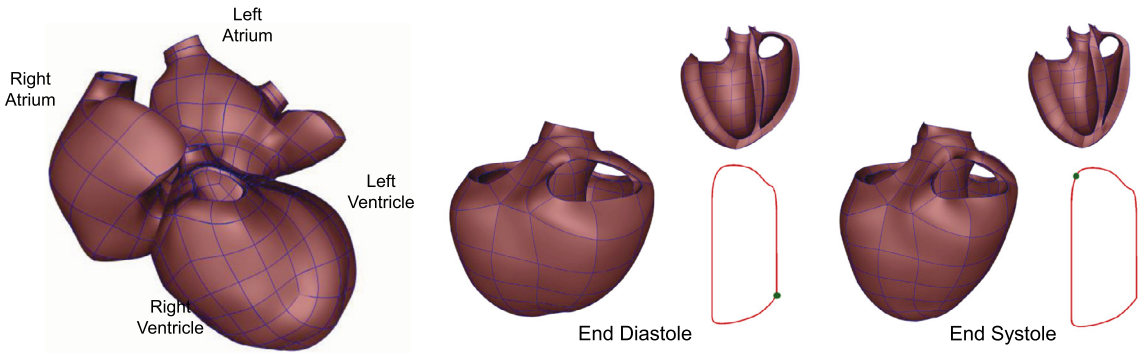

(a) Four Chamber Model (b) Biomechanics Simulation of a Cardiac Cycle

Fig. 1. Topologically complex four-chamber model and a ventricular model with valve annuli at the end-diastolic and end-systolic states of the cardiac cycle. A cut-section (top) and a PV-loop (bottom) are shown inset.

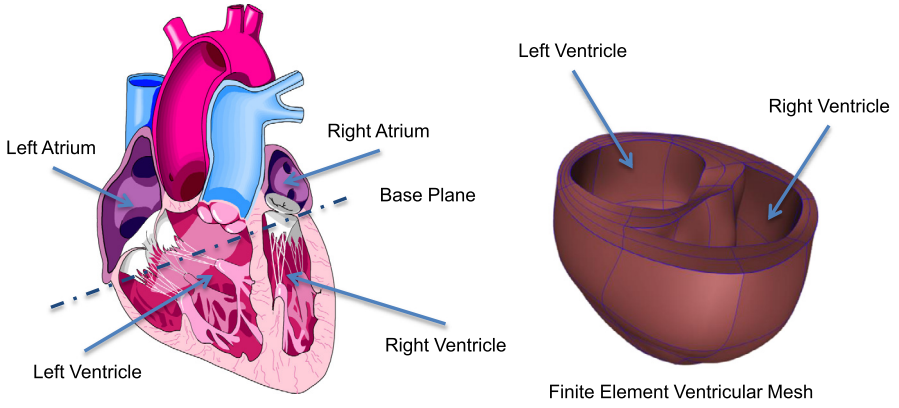

Fig. 2. Cubic-Hermite cardiac finite element meshes have previously been used for modeling ventricular geometry that do not include the valve annuli or the atria.

dinates that are topologically equivalent to a cylinder (Vetter and McCulloch, 1998). However, such meshes require special boundary conditions at the cardiac apex to enable multiple overlapping nodes or "sector" elements (Bradley et al., 1997) to close the mesh. The restriction of using a single set of parametric coordinates enables enforcing continuity across element edges easier, but introduces element distortions.

Gonzales et al. (2013) removed the restriction of having a single set of parametric coordinates in the mesh. The mesh is discretized into a number of sub-regions, each with its own set of parametric coordinates. However, this introduces nodes with an irregular number of neighboring elements, known as extraordinary nodes, at the interface between the sub-regions. Extraordinary nodes are routinely used in linear hexahedral meshes. However, in high-order meshes, enforcing smoothness (i.e., C^0, G^1, or C^1 continuity) conditions along edges incident on extraordinary nodes becomes complicated. Gonzales et al. (2013) described new methods for constructing high-quality bicubic and tricubic Hermite finite element meshes of the human atria. Their meshes preserved smoothness between cubic Hermite elements by introducing an ensemble coordinate frame centered on the nodes and using a generalized local-to-global mapping to transform the derivatives. They used this mapping to construct static finite element meshes of the human atria that can be used to perform non-deforming electrophysiology simulations. We make use of the same mapping in this paper to create finite-element meshes of a four-chamber heart and cardiac ventricles with valve annuli. In addition, we extend the mapping to displacements and coordinate frames, to perform deforming biomechanics simulations using these finite-element meshes.

Cardiac biomechanics simulations make use of the finite strain theory to model deformation of the myocardial tissue. This is because the tissue undergoes large deformations during the cardiac cycle. In addition, the tissue properties are non-linear and anisotropic; the cardiac muscle tissue is stiffer along the axial direction of the cells called the fiber direction. Hence, the constitutive models used for cardiac mechanics make use of hyperelastic, exponential stress-strain relationships with the parameters being different for the fiber and the two cross-fiber directions. In order to capture these large deformations accurately, the displacements of the nodes in the deformable mesh need to be consistently mapped across extraordinary nodes. We make use of the local-to-global mapping used for the geometry to map the global displacements to the local coordinate frame.

Please cite this article in press as: Krishnamurthy, A., et al. Biomechanics simulations using cubic Hermite meshes with extraordinary nodes for isogeometric cardiac modeling. Comput. Aided Geom. Des. (2016), http://dx.doi.org/10.1016/j.cagd.2016.02.016

The cardiac cells in the myocardium are oriented in specific directions across the cardiac wall. The orientation follows a helical pattern from the outside epicardial surface to the inside endocardial surface. In simple ventricular models, this helical orientation can be easily described using a single angle with respect to the circumferential direction of the ventricle. However, using a single fiber angle to describe the fiber direction introduces discontinuity in the direction vectors across edges that are incident on extraordinary nodes. In addition, the fiber angles themselves cannot be converted to the local element coordinates directly using the local-to-global map since the local element parametric directions are not consistent across different regions in meshes with extraordinary nodes. Hence, we convert the fiber angles to local orthogonal coordinate frames and then use the local-to-global map to convert these to consistent fiber directions across element boundaries. However, the use of coordinate frames instead of fiber angles also necessitates the use of a different method for interpolating coordinate frames within the element to capture the changes in the fiber direction smoothly. We make use of the smooth interpolation of coordinate frames in the log-Euclidean space. The coordinate frame is converted to the log-Euclidean space by taking its matrix logarithm, interpolated linearly, and converted back to Euclidean space using the matrix exponential.

In this paper, we extend the generalized local-to-global mapping to perform isogeometric biomechanics simulations with cubic-Hermite meshes that have extraordinary nodes. The main contributions of the paper include:

- Extending the local-to-global mapping to map displacements and fiber directions in the local elements.
- Methods to construct the element stiffness matrices in local element coordinates using the local-to-global mapping (using global perturbations) in meshes with extraordinary nodes.
- Assembling the element stiffness matrices to create a global stiffness matrix in ensemble coordinates.
- Evaluating the computational error and convergence of solution in simple meshes with extraordinary nodes.
- Application of the methods to perform biomechanics simulations in ventricular models with valve annuli and in four-chamber cardiac models.

2. Related and previous work

Cubic-Hermite meshes have been popular in isogeometric finite element analysis, since the representation allows all DOFs to be concentrated at the element corners, without the need for element edge or body nodes. This simplifies the topology or the connectivity information of cubic-Hermite meshes when compared to cubic-Bézier patches, even though both representations are equivalent. In addition, all mathematical derivations that use cubic-Bézier patches are also valid for cubic-Hermite patches. Several researchers have derived the conditions for continuity of piecewise polynomial surface patches; we just list a few that were used to motivate the current work. The paper by DeRose (1990) and the review by Du and Schmitt (1990) derive the conditions for G^1 continuity for cubic-Bézier patches in the presence of extraordinary nodes. Che et al. (2005), Wang and Zhang (2010) extend the discussion to include continuity of adjacent NURBS surfaces.

Isogeometric analysis using NURBS surfaces and basis functions were first developed by Hughes et al. (2005) for general finite element analysis. However, the method developed by Nielsen et al. (1991) for modeling cardiac geometry and mechanics can be considered isogeometric analysis since the same cubic-Hermite basis functions were used to interpolate the cardiac geometry and the finite element dependent variable. The methods developed by Nielsen et al. (1991) were restricted to meshes that have only regular nodes. This work extends the finite element analysis to meshes that have extraordinary nodes. We make use of the general framework developed by Gonzales et al. (2013) to construct cubic-Hermite meshes with extraordinary nodes and extend it to perform biomechanics simulations.

Cubic-Hermite elements have been shown to have better convergence properties compared to linear hexahedral or tetrahedral elements in cardiac electrophysiology simulations. Vincent et al. (2015) compared the convergence behavior of linear Lagrange, cubic-Hermite, and cubic Hermite-style serendipity interpolation methods for finite element simulations of cardiac electrophysiology in static meshes. They found that the high-order methods reach converged solutions with fewer degrees of freedom and longer element edge lengths than traditional linear elements. Recently, Kapl et al. (2015) reported that optimal convergence in isogeometric finite element analysis occurs for bilinear two-patch geometries and C^1 splines of polynomial degree at least 3. Extending on this result, Collin et al. (2015) inferred that optimal convergence of C^1 isogeometric spaces occur with analysis-suitable G^1 geometry parametrizations. In our simulations, we expect the same convergence advantages of cubic-Hermite elements over linear hexahedral or tetrahedral elements in biomechanics simulations with deforming meshes.

Subdivision has been extensively used in computer graphics and animation to overcome the difficulty of enforcing continuity across adjacent surface patches. In addition, the continuity of subdivision surfaces around extraordinary nodes has been well characterized (Doo and Sabin, 1978; Catmull and Clark, 1978). However, the use of subdivision surfaces has been limited in finite element analysis. Gonzales et al. (2013) make use of the Li–Kobbelt interpolatory subdivision scheme (Li et al., 2005) as an intermediate step to calculate the local element derivatives. In addition, for estimating the internal derivatives of cubic Hermite volumes, a volume subdivision scheme such as the one developed by Bajaj et al. (2002) is required. We briefly explain the methods used to estimate the cubic-Hermite derivatives in this paper.

There have been detailed histological studies (Streeter et al., 1969; LeGrice et al., 1995; Costa et al., 1999) in isolated canine specimens to measure the anisotropic structure of the myocardium. The myocardium consists of a mesh of myofibers embedded in laminar sheets separated by cleavage planes. Statistical analysis of fiber architecture variation in a population of human hearts has revealed that fiber orientations are well preserved between individuals (Lombaert et al., 2011). This

Please cite this article in press as: Krishnamurthy, A., et al. Biomechanics simulations using cubic Hermite meshes with extraordinary nodes for isogeometric cardiac modeling. Comput. Aided Geom. Des. (2016), http://dx.doi.org/10.1016/j.cagd.2016.02.016

suggests that the fiber orientations in a human heart can be modeled using measurements from normal adult humans after accounting for variations in ventricle size and shape. The fiber angles in the epicardial (outside) surface of normal hearts are measured to be -60° to the circumferential direction, while they are measured to be 60° to the circumferential direction in the endocardial (inside) surface. The fiber angles across the ventricular wall usually vary linearly between these two angles.

To overcome the problems associated with interpolation of fiber angles in meshes with extraordinary nodes, we make use of a coordinate-frame interpolation. This is mathematically similar to interpolation of tensor fields. However, interpolating tensor fields in normal Euclidean space results in null or non-positive-definite interpolated tensors (Fillard et al., 2006) that are not representative of coordinate frames. Affine invariant Riemannian frameworks have been proposed which overcome these artifacts but are computationally expensive (Pennec et al., 2006). In this paper, we make use of tensor interpolation using a log-Euclidean framework. This method has the advantage of being simpler to implement using our existing cubic Hermite interpolation framework, while preserving the orthogonality of the interpolated coordinate frame (Arsigny et al., 2005).

Newer imaging techniques such as diffusion-tensor magnetic resonance imaging (DT-MRI) can be used to image the fiber directions of the muscles in the ventricular walls directly. Comparing histological measurements of the orientation of muscle fibers and sheets with DT-MRI measurements have confirmed that the fiber and sheet-normal directions coincide with the primary (Hsu et al., 1998; Holmes et al., 2000; Scollan et al., 2000) and tertiary (Helm et al., 2005) eigenvectors of the diffusion tensors. Hence, our method of tensor interpolation in the log-Euclidean frame can also be used to interpolate the fiber-sheet directions in a model of the ventricle with a set of local orthogonal material coordinate axes calculated from measured diffusion tensors.

3. Review of cubic Hermite interpolation

In this section, we provide a summary of the geometric interpolation for extraordinary nodes developed by Gonzales et al. (2013). This section has been included in this paper for completeness. In Section 5, we make use of this interpolation method and extend it to perform biomechanics finite element analysis with deforming meshes.

Cubic-Hermite hexahedral finite element meshes are tri-variate brick volumes with 8 nodes, where each of the six faces consist of a cubic-Hermite surface patch. The element nodes have 8 element degree of freedom (DOF): the value, 3 first derivatives, 3 second cross-derivatives, and 1 triple derivative. In rectangular Cartesian coordinates for geometry and biomechanics simulations, there are 3 coordinates for each DOF. Hence, for biomechanics problems, each element has 8 nodes $\times$ 8 DOF $\times$ 3 Coordinates $=$ 192 DOFs. In 3D cubic-Hermite isogeometric finite element analysis, the geometry and the dependent variables (nodal displacements in mechanics) are interpolated using the same trivariate basis functions Ψ^i, $i = 1 \ldots 64$,

$$\mathbf{x} = \sum_{i=1}^{64} \mathbf{x}_i \Psi_i(\xi_1, \xi_2, \xi_3). \tag{1}$$

The basis functions are obtained as the product of 3 univariate cubic-Hermite basis functions: one for each direction,

$$\Psi_{ijk}(\xi_1, \xi_2, \xi_3) = \Phi_i(\xi_1)\Phi_j(\xi_2)\Phi_k(\xi_3). \tag{2}$$

These equations are used to interpolate the dependent variable at the parametric point (ξ_1, ξ_2, ξ_3) in the world coordinate frame (x_1, x_2, x_3).

In meshes with no extraordinary nodes, the continuity preserved at regular nodes (4 adjacent elements in 2D and 8 adjacent elements in 3D) since nodal DOFs are shared. Bradley et al. (1997) showed that G^1 continuity is preserved across adjacent elements as long as the nodal derivatives are shared by nodes of the adjacent elements. In addition, they introduced a scalar scale factor, S_i, for each element node,

$$\left(\frac{d\mathbf{x}}{d\xi_i}\right)_{ne} = \left(\frac{ds}{d\xi_i}\right)_e \left(\frac{d\mathbf{x}}{ds}\right)_{NG}, \tag{3}$$

$$S_i = \left(\frac{ds}{d\xi_i}\right), \tag{4}$$

which when multiplied with the unit nodal derivative, preserved C^1 continuity. If the scale factor is chosen as the length of the incident edges, then C^1 continuity is enforced based on the arc-length parametrization. This makes physical sense for finite element analysis, since the continuity is independent of the parametrization used for interpolation.

In Equation (3), the subscript *ne* corresponds to the local element derivative at the element node while the subscript *NG* stands for the global node number. In addition to the scalar scale factors for the first derivatives, the scalar scale factors for the mixed second derivatives and the third derivative can be computed as product of the corresponding first derivative scale factors using

$$S_{ij} = \left(\frac{d^2 s}{d\xi_i d\xi_j}\right) = S_i S_j. \tag{5}$$

Please cite this article in press as: Krishnamurthy, A., et al. Biomechanics simulations using cubic Hermite meshes with extraordinary nodes for isogeometric cardiac modeling. Comput. Aided Geom. Des. (2016), http://dx.doi.org/10.1016/j.cagd.2016.02.016

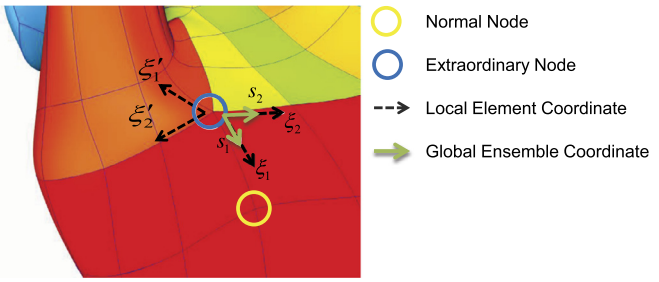

Fig. 3. An ensemble (global) coordinate frame centered on each node is used to maintain continuity of geometry and solution fields across adjacent elements. (For interpretation of the colors in this figure, the reader is referred to the web version of this article.)

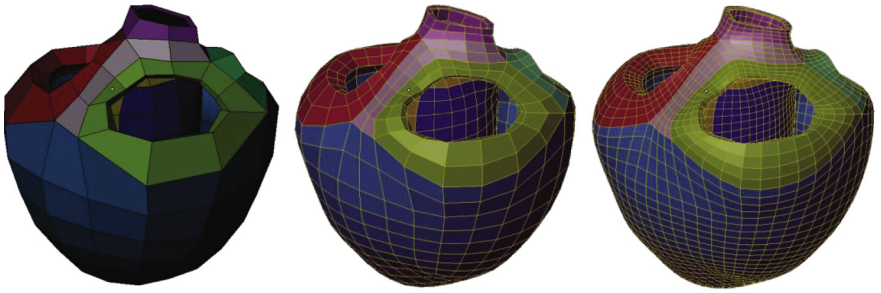

Fig. 4. The cubic Hermite derivatives around extraordinary nodes are estimated by subdividing the mesh twice and using the resulting mesh to calculate the local element derivatives.

3.1. Cubic Hermite interpolation with extraordinary nodes

The same parametric direction cannot be used to interpolate within the elements on either side of an element edge incident on an extraordinary node. As a result, even maintaining C^0 continuity is difficult since it is not possible to share the local element derivative directions using only a scalar scale factor at an extraordinary node. In order to maintain continuity, Gonzales et al. (2013) introduced a new coordinate frame centered on each node, called the ensemble coordinates, and constructed a generalized local-to-global map to transform the global ensemble derivatives to the local element derivatives.

The ensemble frame is shown in green in Fig. 3 and is denoted by s. The parametric directions from one of the elements surrounding the extraordinary node are used to construct the ensemble frame. The generalized local-to-global map is then used to convert the global ensemble derivatives to the local element derivatives using

$$\left(\frac{\partial \mathbf{x}}{\partial \xi_i}\right)_{ne} = \sum_{j=1}^{3} \left(\frac{\partial s_j}{\partial \xi_i}\right)_e \left(\frac{\partial \mathbf{x}}{\partial s_j}\right)_{NG}, \tag{6}$$

$$\mathbf{S}_e = \begin{bmatrix} \frac{\partial s_1}{\partial \xi_1} & \frac{\partial s_2}{\partial \xi_1} & \frac{\partial s_3}{\partial \xi_1} \\ \frac{\partial s_1}{\partial \xi_1} & \frac{\partial s_2}{\partial \xi_1} & \frac{\partial s_3}{\partial \xi_1} \\ \frac{\partial s_1}{\partial \xi_1} & \frac{\partial s_2}{\partial \xi_1} & \frac{\partial s_3}{\partial \xi_1} \end{bmatrix}. \tag{7}$$

The second and third-order mixed derivatives are selected from the element whose derivatives are chosen to coincide with the ensemble frame. The local-to-global transformation map for these higher-order derivatives are constructed from the first-order derivatives using the chain rule

$$\left(\frac{\partial^2 \mathbf{x}}{\partial \xi_i \partial \xi_j}\right)_{ne} = \sum_{k=1}^{3}\sum_{l=1}^{3} \left(\frac{\partial s_k}{\partial \xi_i}\right)_e \left(\frac{\partial s_l}{\partial \xi_j}\right)_e \left(\frac{\partial^2 \mathbf{x}}{\partial s_k \partial s_l}\right)_{NG}, k \neq l. \tag{8}$$

In order to maintain continuity, the local element derivative along the shared edge of both adjacent elements needs to be the same. Enforcing this in practice while constructing complex finite element meshes is tedious. To make the process tractable, Gonzales et al. (2013) used an interpolatory subdivision scheme developed by Li et al. (2005) to subdivide the meshes twice (Fig. 4). The nodes from the twice-subdivided mesh are then used to estimate the local element derivatives. It is also possible to perform exact evaluation of the derivatives by computing the limit surface of the subdivision mesh. However, in practice, it is easier to estimate the derivatives from the twice-subdivided mesh to enforce C^0 continuity.

Please cite this article in press as: Krishnamurthy, A., et al. Biomechanics simulations using cubic Hermite meshes with extraordinary nodes for isogeometric cardiac modeling. Comput. Aided Geom. Des. (2016), http://dx.doi.org/10.1016/j.cagd.2016.02.016

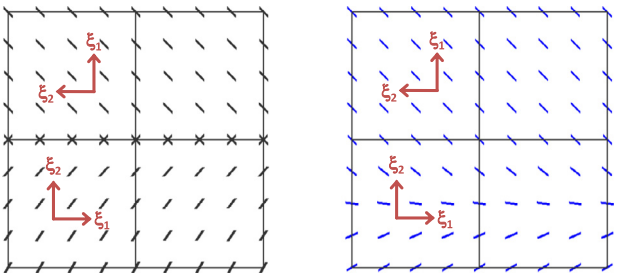

(a) Fiber Angle Interpolation (b) Coordinate Frame Interpolation

Fig. 5. Interpolation of fiber angles in meshes with inconsistent parametric direction results in fiber direction discontinuity along the region boundaries. To prevent this, we interpolate the coordinate frames using log-Euclidean transformation resulting in smooth interpolation of fiber directions.

Since the subdivided nodes are shared between the elements that share element edges, C^0 continuity is enforced along all element edges, including those incident on extraordinary nodes. In addition, G^1 continuity could be enforced in the local region surrounding an extraordinary node if the subdivided nodes are coplanar. G^1 continuity along element edges is enforced if the subdivided nodes on either side of the edge are collinear with the shared edge node. Please refer to the review by Du and Schmitt (1990) for the necessary and sufficient conditions to enforce G^1 continuity with Bézier patches. The same conditions can be extended to cubic-Hermite patches with extraordinary nodes since cubic-Hermite representation is equivalent to the cubic-Bézier representation.

4. Interpolation of fiber directions

We make use of a coordinate-frame interpolation of fiber directions to ensure smooth interpolation of the fiber directions in the presence of extraordinary nodes. In modeling the fiber architecture of the atria, Gonzales et al. (2013) used a fixed fiber angle for each region that were based qualitatively on published diagrams of atrial fiber tracts, since measuring the fiber angles in the atria is difficult owing to their thin walls. Hence, an interpolation method was not needed for the atria, since the transmural variation of fiber directions in the atria was not modeled. However, in the cardiac ventricles, the fiber directions vary significantly in the transmural direction, which necessitates a method for interpolation. In this section, we describe a coordinate-frame interpolation method based on the log-Euclidean transformation (see Fig. 5).

The coordinate frame corresponding to the fiber and cross-fiber directions at each nodal location is represented using a 3×3 orthogonal matrix, $\mathbf{F}$ whose columns represent the vectors along the three orthonormal coordinate directions. In order to interpolate the coordinate frame, we convert it to the log-Euclidean space by taking the matrix logarithm. However, for the matrix logarithm to be real, the matrix needs to be invertible and each Jordan block belonging to a negative eigenvalue occurs an even number of times. In order to satisfy this condition for any coordinate frame, we construct a synthetic symmetric matrix, $\mathbf{T}$, with synthetic but unique and positive eigenvalues, using eigen composition as shown below,

$$\mathbf{T} = \mathbf{F} \begin{bmatrix} d_{11} & 0 & 0 \\ 0 & d_{22} & 0 \\ 0 & 0 & d_{33} \end{bmatrix} \mathbf{F}^T. \tag{9}$$

In Equation (9), the values of d_{11}, d_{22}, and d_{33} are chosen to be unique, positive, and in sorted order ($d_{11} < d_{22} < d_{33}$, $(5, 10, 20)$, for example). The matrix logarithm $\mathbf{L}$ of the matrix $\mathbf{T}$,

$$\mathbf{L} = \log(\mathbf{T}), \tag{10}$$

is then used to interpolate the coordinate frames within an element. The matrix logarithm of a positive definite matrix is symmetric and hence, has only six independent components. We make use of the same basis function values as the geometry to interpolate the components of $\mathbf{L}$, similar to scalar quantities in Euclidean space. The fiber coordinate interpolation takes advantage of the local-to-global mapping to interpolate the six independent components of $\mathbf{L}$. At any evaluation point inside the element, the coordinate frame can then be computed by computing the matrix exponential of the interpolated $\mathbf{L_e}$,

$$\mathbf{T_e} = e^{(\mathbf{L_e})}, \tag{11}$$

and then computing the eigenvectors, v_i $(i = 1, 2, 3)$ of the resulting matrix. The eigenvalues of $\mathbf{T_e}$ are then used to sort the eigenvectors to make sure that the order of vectors in the coordinate frame is preserved. Since the eigenvalues are only used for sorting the eigenvectors, there are no stability issues during interpolation as long as they are positive and unique.

5. Finite element analysis with extraordinary nodes

Performing mechanics finite element simulations on meshes with extraordinary nodes require three key modifications to the cubic-Hermite finite element formulation. The first modification deals with a local-to-global mapping of global pa-

Please cite this article in press as: Krishnamurthy, A., et al. Biomechanics simulations using cubic Hermite meshes with extraordinary nodes for isogeometric cardiac modeling. Comput. Aided Geom. Des. (2016), http://dx.doi.org/10.1016/j.cagd.2016.02.016

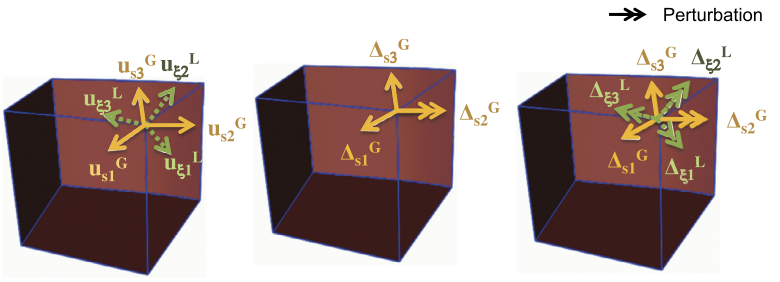

Fig. 6. To compute the element stiffness matrix, the global perturbation in the ensemble coordinate frame is transformed to the local element coordinates using the inverse of the local-to-global transformation map.

rameters and dependent variables. The second modification is to the perturbations used to calculate the element tangent stiffness matrix. The final modification is to use the local-to-global mapping to assemble the global stiffness matrix from the element stiffness matrices.

In Section 3.1, the generalized local-to-global mapping is used to map the local element derivatives to the ensemble derivatives. The finite element equations are solved with values in the ensemble frame as the dependent variables. It can be noted that the local-to-global mapping for all DOFs (first derivatives, second and third mixed derivatives) are linear. This suggests that the local-to-global mapping can be represented using a single matrix of size $n \times n$, where n is the number of DOFs at each element node. Going further, the transformations for all 8 element nodes can be combined to a single transformation map that converts the local element DOF to the global ensemble DOF at the global node. This unification of the local-to-global map simplifies the equations for converting the values of the dependent variables in the ensemble frame to the local element coordinate frame using

$$[\mathbf{u}]_L = [\Gamma]_e \, [\mathbf{u}]_G \, . \tag{12}$$

In Equation (12) the local-to-global map is represented as Γ, and $\mathbf{u}$ corresponds to the element DOFs. This generalized local-to-global mapping directly maps the element DOF to the ensemble DOF $\mathbf{u}_G$ at the corresponding global nodes. The local-to-global transformation map is invertible as long as the first derivatives in the local or the global ensemble frames are not degenerate.

5.1. Element stiffness matrix calculation

In our cubic-Hermite finite element formulation, the equilibrium geometry (nodal deformations) is computed using Newton iteration. The tangent stiffness matrix for the whole system at the current deformed configuration is computed and is then solved using Newton iteration. This is performed by first computing the local element tangent stiffness matrices and then assembling them to compute the global tangent stiffness matrix.

The element tangent stiffness matrix is calculated using finite difference by perturbing the current deformed degrees of freedom and recalculating the resulting residual forces. This perturbation needs to be performed with respect to the global ensemble frame in order to apply the same deformations to the local element nodes belonging to neighboring elements that share the global node. In a mesh with only regular nodes, perturbing the global degrees of freedom is equivalent to a constant multiple of the same perturbation in the local coordinate frame; it is scaled by the scalar scale factor (Section 3). In the presence of extraordinary nodes, the global perturbations have to be converted to local perturbations for each element adjacent to the extraordinary node. This is achieved by applying the inverse of the local-to-global transformation map to the perturbation using

$$[\Delta]_G = [\Gamma]_e^{-1} \, [\Delta]_L \, . \tag{13}$$

Fig. 6 shows an example of mapping the deformations of the first derivative DOF. The perturbation in the global ensemble frame shown in the middle is transformed to the local element frame as shown in the right using the inverse of the local-to-global transformation map. After the perturbations are transformed to the local element coordinate frame, the element stiffness matrix is computed as before using finite difference.

5.2. Global stiffness matrix assembly

The element stiffness matrices computed using the method explained in Section 5.1 are in the local element coordinate frame. However, the components of the global tangent stiffness matrix are in the ensemble frame for each global node. The final step required for including extraordinary nodes is to convert the element stiffness matrix values from the local coordinate frame to the global ensemble frame. Again, we make use of the general local-to-global mapping to convert the stiffness values to the global coordinate frame. We apply the transformation to the residual forces that are the result of the perturbations to convert them to the global coordinate frame, which are then used for assembly.

Please cite this article in press as: Krishnamurthy, A., et al. Biomechanics simulations using cubic Hermite meshes with extraordinary nodes for isogeometric cardiac modeling. Comput. Aided Geom. Des. (2016), http://dx.doi.org/10.1016/j.cagd.2016.02.016

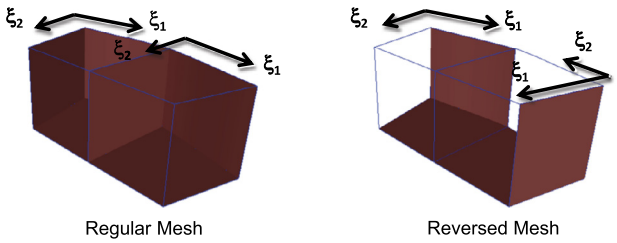

Fig. 7. Two simple meshes consisting of 2 cubic-Hermite elements were constructed to evaluate the correctness of the local-to-global mapping. The local parametric directions were not consistent in the second mesh.

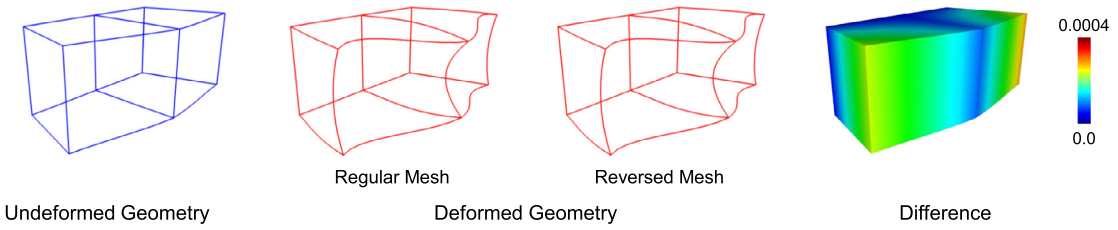

Fig. 8. The deformation in both meshes were similar to within the tolerance used for the simulation (0.001) ensuring that the solution is independent of the direction of the local parametrization. For interpretation of the colors in this figure, the reader is referred to the web version of this article.

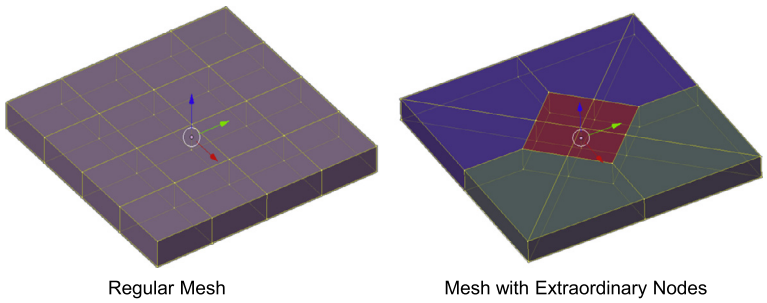

Fig. 9. Two meshes of cuboid geometry; the first consisting of only regular nodes and the second consisting of 8 extraordinary nodes.

The assembly of the global stiffness matrix is straightforward after converting the element stiffness matrix components to the global ensemble frame since the residual forces are with respect to the common global ensemble coordinate frame. Finally, after assembling, the global system is solved using Newton method for the dependent variables (nodal deformations) that are also in the global coordinate frame.

6. Finite element analysis of simple meshes

Two tests were performed on simple meshes to analyze the correctness of the solution as well as to compute the errors due to the presence of extraordinary nodes.

To estimate the correctness of the local-to-global mapping in the presence of a change in the interpolating variable, two simple meshes consisting of 2 cubic-Hermite elements were constructed. Both meshes had the same geometric location of the nodes; however, the parametric directions were reversed in one element of the second mesh making the parametric directions inconsistent (Fig. 7). The same boundary conditions were then applied to both meshes and the deformed geometry was calculated using the new finite element methods described in this paper. The two resulting deformed geometries were then compared and the deformations were found to be the same to within the tolerance used for the simulation (0.001). The spatial variation of the difference in the displacement solution between the regular and reversed mesh is shown in Fig. 8. In addition, both the meshes took the same number of iterations to converge to the solution. This shows that the global solution is independent of the local element parametrization.

To understand the errors in the solution in the presence of extraordinary nodes, two meshes of a simple cuboid geometry were constructed. The first mesh was constructed using 16 elements and 50 regular nodes, while the second mesh was constructed using 12 elements with 34 nodes of which 8 nodes were extraordinary (Fig. 9). The nodes of the meshes at one end were fixed and the nodes in the opposite end were pulled to deform the geometry. The top view of the deformed geometry is shown in Fig. 10.

Please cite this article in press as: Krishnamurthy, A., et al. Biomechanics simulations using cubic Hermite meshes with extraordinary nodes for isogeometric cardiac modeling. Comput. Aided Geom. Des. (2016), http://dx.doi.org/10.1016/j.cagd.2016.02.016

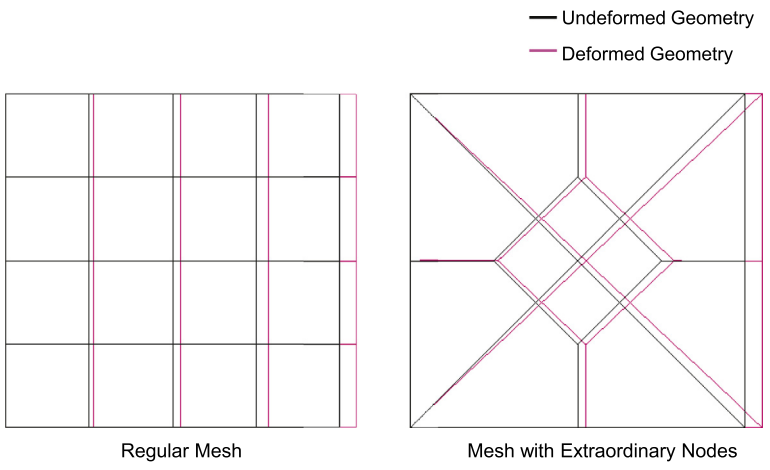

Fig. 10. Top-view of the deformation of the two cuboid meshes.

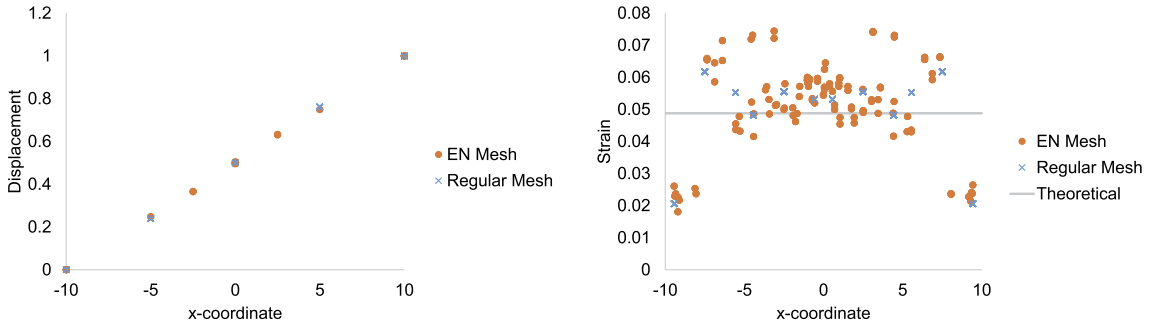

(a) Nodal Displacement (b) Strain

Fig. 11. Scatter plot of the nodal deformation with respect to the x-coordinate and the Scatter plot of the strains calculated at Gauss points with respect to the x-coordinate of the Gauss point.

To compare the solution obtained in both cases, a scatter plot showing the nodal displacements at their corresponding x-coordinate is shown in Fig. 11(a). In addition, a scatter plot of the calculated strain values at the Gauss points for both meshes is shown in Fig. 11(b). It can be seen that while the nodal displacements are very similar in both cases, the standard deviation in the strain values is higher in the case with extraordinary nodes. However, the values are still within the error tolerances in both cases ($< 5\%$).

We compared the effect of the presence of extraordinary nodes on the convergence of results in the simple meshes. We compared the convergence of the regular mesh using both cubic-Hermite elements and linear hexahedral elements to the convergence of the cubic-Hermite mesh with extraordinary nodes. The convergence properties were measured by counting the number of newton iterations the simulations took to obtain a solution with an error lower than the user-defined convergence value. It can be seen that the cubic-Hermite mesh converges the fastest, in spite the mesh having many more DOFs (1200). The presence of extraordinary nodes did not significantly affect the convergence, and the mesh with extraordinary nodes consistently converged to the solution within a few extra iterations than the mesh with regular cubic-Hermite elements (see Fig. 12). On the other hand, the linear mesh was consistently slower to converge even with fewer DOFs (150). These results show that the convergence advantages of cubic-Hermite elements are retained for biomechanics simulations in the presence of extraordinary nodes.

7. Application to cardiac modeling

7.1. Complex cardiac models

Using the local-to-global mapping, an anatomically accurate, four-chamber finite element mesh of the heart was generated from segmented CT images (Fig. 1(a)). The model includes all the orifices and valve annuli that are present in a regular heart. It consists of 474 cubic-Hermite elements and 958 nodes. A bi-ventricular model with the four valve annuli was created using the same method (Fig. 1(b)). In addition, biomechanics simulations were then performed using this mesh. This mesh consists of 162 cubic-Hermite elements and 332 nodes. Both meshes were constructed in the software Blender using normal cardiac dimensions, similar to the methods described by Krishnamurthy et al. (2015). A plugin for Blender was

Please cite this article in press as: Krishnamurthy, A., et al. Biomechanics simulations using cubic Hermite meshes with extraordinary nodes for isogeometric cardiac modeling. Comput. Aided Geom. Des. (2016), http://dx.doi.org/10.1016/j.cagd.2016.02.016

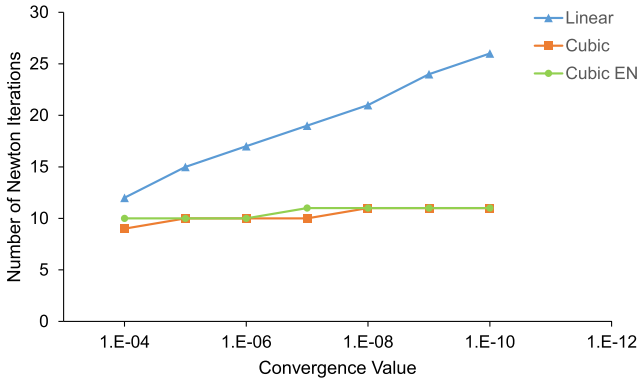

Fig. 12. The presence of extraordinary nodes did not significantly alter the convergence of results on the simple meshes. The mesh with the extraordinary nodes usually converged to the user-defined convergence value within one extra newton iteration when compared to the cubic-Hermite mesh.

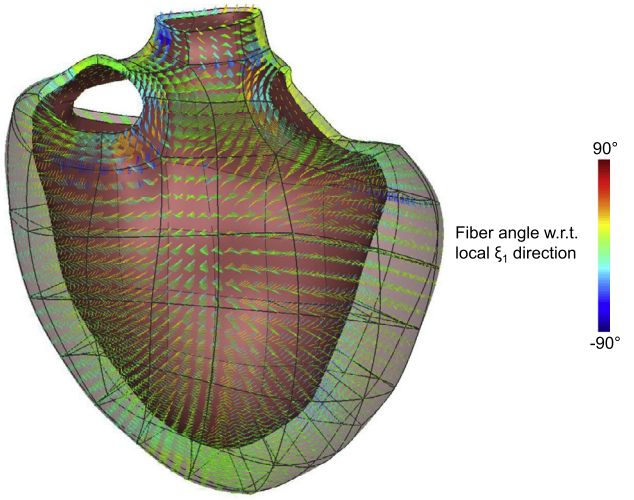

Fig. 13. Fiber directions rendered at different locations in a ventricular model of the heart with valve annuli. The sprites are colored based on the angle with respect to the local parametric direction. For interpretation of the colors in this figure, the reader is referred to the web version of this article.

implemented to perform the subdivision and estimate the nodal derivatives. It can be seen that the use of cubic-Hermite elements along with extraordinary nodes allows for compact representation of complex cardiac models with fewer elements.

7.2. Fiber directions in cardiac models

The coordinate frame interpolation was used to model the fiber direction in the ventricular model with valve annuli. A rule-based approach was used to model the fibers; the outside epicardial surfaces were assigned $-60°$ with respect to the circumferential direction and the inside endocardial surface were assigned $+60°$ with respect to the circumferential direction. Fig. 13 shows the fiber directions in a human cardiac ventricle represented as sprites. The fiber directions follow a left-handed helical pattern from outside to inside. The use of coordinate frame interpolation results in smooth variation in the fiber direction throughout the myocardial tissue.

In Fig. 13, the sprites are colored with respect to the local parametric direction ξ_1. However, along the edges that are incident on extraordinary nodes, there is no consistent local parametric direction on either side. Hence, this coloring does not appear to be consistent. However, it can be seen that the interpolated direction represented by the sprites transition smoothly across these edges that are incident upon extraordinary nodes.

7.3. Simulation of full cardiac cycle in a ventricular model

A complete cardiac cycle was simulated by coupling the bi-ventricular finite element mesh with a lumped-parameter closed-loop circulation model using the methods described in Krishnamurthy et al. (2013). The valve annuli were fixed from moving along the long axis (vertical direction) of the heart. In addition, certain nodes on the outer ring of the four valve annuli were constrained to prevent rigid body motion. After constraining the nodes, pressure boundary conditions corresponding to the left and right ventricular pressures were applied to the inner surfaces of both ventricles. To simulate cardiac

Please cite this article in press as: Krishnamurthy, A., et al. Biomechanics simulations using cubic Hermite meshes with extraordinary nodes for isogeometric cardiac modeling. Comput. Aided Geom. Des. (2016), http://dx.doi.org/10.1016/j.cagd.2016.02.016

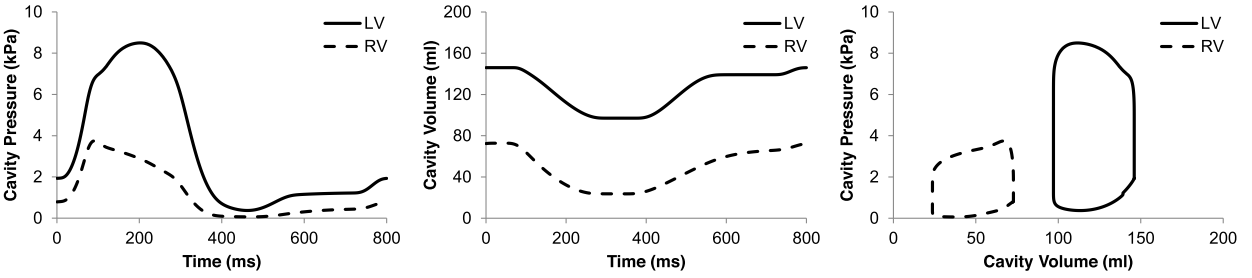

(a) Pressure (b) Volume (c) PV Loop

Fig. 14. Pressure and volume time-course output from the full beat simulation of the bi-ventricular heart model with valve anulli. (c) Shows the simulated pressure-volume loops for the left and right ventricles.

contraction, active forces (tension) were produced internally in the elements and were used to solve for the equilibrium geometry. The equilibrium geometry at each time-step was solved using the finite element analysis methods described in this paper and the resulting nodal solution was output at each time-step.

The resting properties of the myocardium were modeled using the transversely-isotropic form of the constitutive model developed by Holzapfel and Ogden (2009). In this model, the anisotropy in the fiber and cross-fiber directions of the myocardium is modeled using a separate exponential term with different exponents. The strain energy in this model is given by

$$\psi = \frac{a}{2b} e^{b(I_1-3)} + \frac{a_f}{2b_f}\left(e^{b_f(I_{4f}-1)^2} - 1\right). \tag{14}$$

In Equation (14), I_1 corresponds to the first invariant of the right Cauchy–Green strain tensor, I_{4f} corresponds to the components of the right Cauchy–Green strain tensor in the fiber direction. The parameter values reported by Krishnamurthy et al. (2013) were used for the simulations in this paper.

The active contraction model developed by Lumens et al. (2009) is used to model the muscle contraction. The pressure boundary conditions to be applied to the inner surfaces of the left and right ventricles were obtained using a lumped-parameter circulation model (Arts et al., 2005). The parameters reported in Krishnamurthy et al. (2013) were again used for both these models. Several cardiac cycles were simulated until the volume changes in both ventricles reached steady state. This happened within 5 full beats in this simulation. Fig. 14(a–b) show the pressure and volume time courses for both ventricles. Fig. 14(c) shows the pressure-volume loops for the left and right ventricles. It can be seen that the volume ejected by both ventricles in each beat is the same. This shows that the simulation has reached steady state.

8. Conclusions

We have developed a method by which we can perform cardiac biomechanics simulations on cubic-Hermite meshes with extraordinary nodes. These meshes are capable of representing complex geometries with fewer elements. This reduces the computational time since computing the element stiffness matrix for each element is the most computationally intensive operation in higher-order finite element analysis. In addition, locally varying quantities such as the fiber direction have been incorporated into these meshes. Using our method, meshes with locally varying properties can be generated and hence, this method can be used to model complex materials such as the muscle tissue.

Compact cubic Hermite meshes are ideally suited for patient-specific cardiac modeling. Since these meshes have fewer degrees of freedom, they can be used to create template meshes from population averaged cardiac dimensions. These template meshes can then be modified using image registration algorithms to create patient-specific cardiac meshes from images obtained using computed tomography (CT) or magnetic resonance (MR) automatically. Since creating an anatomically accurate patient-specific mesh is the most tedious and time-consuming step of the process, using these meshes can significantly reduce the total time for patient-specific modeling.

The finite element method used in this paper only rely on C^0 continuity of geometry and dependent variables between the elements for mechanics simulations. However, the methods used for constructing the cubic-Hermite finite element mesh and the local-to-global mapping are more general and can be used to enforce higher order G^1 continuity by modifying the twice-subdivided mesh suitably. Enforcing high-order continuity might help reduce the total DOFs in the analysis and might improve convergence by requiring fewer iterations to reach a converged solution.

Using anatomically accurate heart models for biomechanics simulations will enable modeling of complex interactions that were not previously possible with ventricular models that do not include the valve plane. One example is to model mitral valve regurgitation by linking it to changes in the mitral valve annuli during the heart cycle. The four-chamber mesh can be used to model the effect of atrial geometry on the heart function. Anatomically accurate boundary conditions can be imposed on the cardiac geometry, resulting in the model replicating the motion of the cardiac walls and the valve plane accurately during the cardiac cycle.

Please cite this article in press as: Krishnamurthy, A., et al. Biomechanics simulations using cubic Hermite meshes with extraordinary nodes for isogeometric cardiac modeling. Comput. Aided Geom. Des. (2016), http://dx.doi.org/10.1016/j.cagd.2016.02.016

Acknowledgements

This work was supported by NIH grants NHLBI 1 R01 HL96544 (ADM), NHLBI 1 RO1 HL091036 (WPS), NHLBI 5 T32 HL007089, NHLBI 1 T32 HL105373, NIBIB 1 T32 EB009380 (ADM), NIGMS 8 P41 GM103426 (National Biomedical Computation Resource).

References

Aguado-Sierra, J., Krishnamurthy, A., Villongco, C., Chuang, J., Howard, E., Gonzales, M.J., Omens, J., Krummen, D.E., Narayan, S., Kerckhoffs, R.C., McCulloch, A.D., 2011. Patient-specific modeling of dyssynchronous heart failure: a case study. Prog. Biophys. Mol. Biol. 107, 147–155.

Arsigny, V., Fillard, P., Pennec, X., Ayache, N., 2005. Fast and simple calculus on tensors in the log-Euclidean framework. In: Medical Image Computing and Computer-Assisted Intervention–MICCAI 2005, pp. 115–122.

Arts, T., Delhaas, T., Bovendeerd, P., Verbeek, X., Prinzen, F., 2005. Adaptation to mechanical load determines shape and properties of heart and circulation: the CircAdapt model. Am. J. Physiol., Heart Circ. Physiol. 288, H1943.

Bajaj, C., Schaefer, S., Warren, J., Xu, G., 2002. A subdivision scheme for hexahedral meshes. Vis. Comput. 18, 343–356.

Bradley, C., Pullan, A., Hunter, P., 1997. Geometric modeling of the human torso using cubic Hermite elements. Ann. Biomed. Eng. 25, 96–111.

Catmull, E., Clark, J., 1978. Recursively generated b-spline surface on arbitrary topological meshes. Comput. Aided Des. 10, 350–355.

Che, X., Liang, X., Li, Q., 2005. G^1 continuity conditions of adjacent NURBS surfaces. Comput. Aided Geom. Des. 22, 285–298.

Collin, A., Sangalli, G., Takacs, T., 2015. Approximation properties of multi-patch C^1 isogeometric spaces. arXiv preprint, arXiv:1509.07619.

Costa, K., Hunter, P., Wayne, J., Waldman, L., Guccione, J., McCulloch, A., 1996. A three-dimensional finite element method for large elastic deformations of ventricular myocardium: II-prolate spheroidal coordinates. J. Biomech. Eng. 118, 464–472.

Costa, K., Takayama, Y., McCulloch, A., Covell, J., 1999. Laminar fiber architecture and three-dimensional systolic mechanics in canine ventricular myocardium. Am. J. Physiol., Heart Circ. Physiol. 276, H595.

DeRose, T.D., 1990. Necessary and sufficient conditions for tangent plane continuity of Bézier surfaces. Comput. Aided Geom. Des. 7, 165–179.

Doo, D., Sabin, M., 1978. Behaviour of recursive division surfaces near extraordinary points. Comput. Aided Des. 10, 356–360.

Du, W.-H., Schmitt, F.J., 1990. On the G^1 continuity of piecewise Bézier surfaces: a review with new results. Comput. Aided Des. 22, 556–573.

Fillard, P., Arsigny, V., Pennec, X., Ayache, N., 2006. Joint estimation and smoothing of clinical DT-MRI with a log-Euclidean metric. Research report RR-5584.

Gonzales, M.J., Sturgeon, G., Krishnamurthy, A., Hake, J., Jonas, R., Stark, P., Rappel, W.J., Narayan, S.M., Zhang, Y., Segars, W.P., McCulloch, A.D., 2013. A three-dimensional finite element model of human atrial anatomy: new methods for cubic Hermite meshes with extraordinary vertices. Med. Image Anal. 17, 525–537.

Helm, P., Beg, M., Miller, M., Winslow, R., 2005. Measuring and mapping cardiac fiber and laminar architecture using diffusion tensor MR imaging. Ann. N.Y. Acad. Sci. 1047, 296.

Holmes, A., Scollan, D., Winslow, R., 2000. Direct histological validation of diffusion tensor MRI in formaldehyde-fixed myocardium. Magn. Reson. Med. 44, 157–161.

Holzapfel, G., Ogden, R., 2009. Constitutive modelling of passive myocardium: a structurally based framework for material characterization. Philos. Trans. R. Soc. Lond. A 367, 3445.

Hsu, E., Muzikant, A., Matulevicius, S., Penland, R., Henriquez, C., 1998. Magnetic resonance myocardial fiber-orientation mapping with direct histological correlation. Am. J. Physiol., Heart Circ. Physiol. 274, H1627.

Hughes, T.J., Cottrell, J.A., Bazilevs, Y., 2005. Isogeometric analysis: CAD, finite elements, NURBS, exact geometry and mesh refinement. Comput. Methods Appl. Mech. Eng. 194, 4135–4195.

Kapl, M., Vitrih, V., Jüttler, B., Birner, K., 2015. Isogeometric analysis with geometrically continuous functions on two-patch geometries. Comput. Math. Appl..

Kerckhoffs, R., Neal, M., Gu, Q., Bassingthwaighte, J., Omens, J., McCulloch, A., 2007. Coupling of a 3D finite element model of cardiac ventricular mechanics to lumped systems models of the systemic and pulmonic circulation. Ann. Biomed. Eng. 35, 1–18.

Kerckhoffs, R., Omens, J., McCulloch, A., Mulligan, L., 2010. Ventricular dilation and electrical dyssynchrony synergistically increase regional mechanical nonuniformity but not mechanical dyssynchrony. Circ. Heart Fail. 3, 528–536.

Krishnamurthy, A., Villongco, C., Beck, A., Omens, J., McCulloch, A., 2015. Left ventricular diastolic and systolic material property estimation from image data. In: Statistical Atlases and Computational Models of the Heart-Imaging and Modelling Challenges. Springer, pp. 63–73.

Krishnamurthy, A., Villongco, C.T., Chuang, J., Frank, L.R., Nigam, V., Belezzuoli, E., Stark, P., Krummen, D.E., Narayan, S., Omens, J.H., et al., 2013. Patient-specific models of cardiac biomechanics. J. Comput. Phys. 244, 4–21.

LeGrice, I., Smaill, B., Chai, L., Edgar, S., Gavin, J., Hunter, P., 1995. Laminar structure of the heart: ventricular myocyte arrangement and connective tissue architecture in the dog. Am. J. Physiol., Heart Circ. Physiol. 269, H571.

Li, G., Ma, W., Bao, H., 2005. A new interpolatory subdivision for quadrilateral meshes. Comput. Graph. Forum 24, 3–16.

Lombaert, H., Peyrat, J., Croisille, P., Rapacchi, S., Fanton, L., Clarysse, P., Delingette, H., Ayache, N., 2011. Statistical analysis of the human cardiac fiber architecture from DT-MRI. In: Functional Imaging and Modeling of the Heart, pp. 171–179.

Lumens, J., Delhaas, T., Kirn, B., Arts, T., 2009. Three-wall segment (TriSeg) model describing mechanics and hemodynamics of ventricular interaction. Ann. Biomed. Eng. 37, 2234–2255.

Niederer, S., Plank, G., Chinchapatnam, P., Ginks, M., Lamata, P., Rhode, K., Rinaldi, C., Razavi, R., Smith, N., 2011. Length-dependent tension in the failing heart and the efficacy of cardiac resynchronization therapy. Cardiovasc. Res. 89, 336–343.

Nielsen, P., LeGrice, I., Smaill, B., Hunter, P., 1991. Mathematical model of geometry and fibrous structure of the heart. Am. J. Physiol., Heart Circ. Physiol. 260, H1365.

Pennec, X., Fillard, P., Ayache, N., 2006. A Riemannian framework for tensor computing. Int. J. Comput. Vis. 66, 41–66.

Scollan, D., Holmes, A., Zhang, J., Winslow, R., 2000. Reconstruction of cardiac ventricular geometry and fiber orientation using magnetic resonance imaging. Ann. Biomed. Eng. 28, 934–944.

Streeter Jr, D., Spotnitz, H., Patel, D., Ross Jr, J., Sonnenblick, E., 1969. Fiber orientation in the canine left ventricle during diastole and systole. Circ. Res. 24, 339.

Vetter, F., McCulloch, A., 1998. Three-dimensional analysis of regional cardiac function: a model of rabbit ventricular anatomy. Prog. Biophys. Mol. Biol. 69, 157–183.

Vincent, K.P., Gonzales, M.J., Gillette, A.K., Villongco, C.T., Pezzuto, S., Omens, J.H., Holst, M.J., McCulloch, A.D., 2015. High-order finite element methods for cardiac monodomain simulations. Front. Physiol. 6.

Wang, W., Zhang, Y., 2010. Wavelets-based NURBS simplification and fairing. Comput. Methods Appl. Mech. Eng. 199, 290–300.

Please cite this article in press as: Krishnamurthy, A., et al. Biomechanics simulations using cubic Hermite meshes with extraordinary nodes for isogeometric cardiac modeling. Comput. Aided Geom. Des. (2016), http://dx.doi.org/10.1016/j.cagd.2016.02.016